Probing Interface Elastic Nonlinearity Applying Nonlinear Resonance Ultrasound Spectroscopy: The Case of Screw Tightness-of-fit

Jacques Rivière,* Guillaume Renaud, Sylvain Haupert, Maryline Talmant, and Pascal Laugier
UPMC Univ Paris 06, CNRS UMR 7623,
Laboratoire d'Imagerie Paramétrique,
F-75006, Paris, France

Paul A. Johnson†
Los Alamos National Laboratory, NM, USA

(Dated: December 21, 2009)

We are exploring various applications of elastic nonlinearity to a number of problems involving interfaces. The aim of this study is to evaluate the sensitivity of Nonlinear Resonance Ultrasound Spectroscopy (NRUS) to torque changes that are reflected in an evolving interface. Our system is comprised of a bolt progressively tightened in an aluminium plate. This apparently simple system is surprisingly complex. Different modes of the system, identified using Finite Element Modelling, are studied in the range 1-25 kHz. These modes mostly correspond to bending modes of the plate. For each mode, nonlinear parameters expressing the importance of resonance frequency and damping variations are extracted. Linear and nonlinear parameters are then compared and their sensitivity is discussed. In addition, the influence of the mode type on the sensitivity of nonlinear parameters is discussed. Results suggest that a multimodal NRUS measurement can be an appropriate and sensitive method for monitoring bolt tightening. Further work must be carried out to apply this method in medical or industrial contexts.

PACS numbers: Valid PACS appear here
Keywords: Multimodal Nonlinear Resonance Ultrasound Spectroscopy, Interface Evolution, Tightening, Loosening, Torque, Finite Element Modelling, Non destructive testing

I. INTRODUCTION

A portion of our work is aimed at exploring the application of elastic nonlinear methods to probe the physics of interfaces, and to study potential applications. In this work we focus in a problem that appears simple on the surface, the tightening of a screw or bolt in a metal plate– but turns out to be highly complex. Widely used in many industrial applications, bolted structures have been a research domain for many years, from conception of these structures to conception of quality control devices of tightening. In the latter domain, ultrasonic methods occupy an important position. Several publications appeared in the 70s using the variation of the first compressional resonance mode of the screw to determine the tightening forces on it, either in the time domain or in the frequency domain[1–4]. In the time domain, a pulse echo system allows to measure the time of flight of a longitudinal wave within the screw. Variation of wave speed gives information on the tightening forces (acoustoelastic effect)[2,4].

At present, a number of research groups have improved upon this measurement. A real time control of tightening has been developped by Nassar *et al.*[5], based on the time domain measurement. Similarly, Chaki *et al.*[6] developped a system combining longitudinal and transversal waves (termed the bi-wave method) to avoid systematic calibrations in industrial applications.

Furthermore, many studies have been performed to detect loosening of rivets, widely used in aeronautics. For example, the combination of thermography and ultrasound techniques enables Zweschper *et al.* to detect flawed rivets[7,8]. The structure is excited by ultrasound, which causes heating of flawed rivets by dissipation. Then, thermography is used to detect heated areas. More generally, methods using Eddy Current[9–11], X-Radiography[12,13], or Magneto-Optic interactions[14,15] are also either in progress or already employed for riveted structures.

In medical domain, Meredith *et al.* developped the RFA method (Resonance Frequency Analysis)[16] in 1996 to assess the stability of a dental implant. A L-shape sensor is fixed to the dental implant after surgery to monitor bone healing. Indeed, the first bending resonance of the 'sensor-implant' system is sensitive to stress exerced by bone surrounding the implant. Similarly, the *Periotest*© device developped by Dhoedt *et al.*[17] in 1985 consists in damping measurements of the implant/bone system by means of a calibrated impact.

Little work has been done in nonlinear acoustics on this subject. Very recent publications[18,19] reported the sum-frequency level ($f_1 + f_2$) created by exciting bolted joints with two sinusoidal waves (f_1 and f_2), for different torque levels. More generally, nonlinear acoustics offers some sensitive techniques to detect an isolated and localized micro-crack[20], as well as to evaluate a global level of micro-damage in materials such as rock[21,22], nickel[23], concrete[24–26], wood[27], bone[28,29], etc. These techniques are mainly based on harmonic generation[30–32], frequency mixing[33–35], acoustoelasticity[36,37] or shift of the reso-

nance frequency[26,28,38,39]. The latter, termed Nonlinear Resonance Ultrasound Spectroscopy (NRUS), provides the means to extract nonlinear elastic and dissipative parameters, associated to changes in the resonance frequency and damping with level of excitation, respectively.
The aim of this study is to evaluate the sensitivity of NRUS to torque changes, in a system composed of a screw tightened in a plate. As nonlinear methods are generally more sensitive than linear ones (velocity and attenuation measurements), we expect to obtain complementary information and/or better sensitivity from these measurements.

II. THEORY

In the framework of linear elasticity, stress and strain are linearly related by a constant elastic modulus. If nonlinearity has to be considered, the Landau theory[40] allows to describe 'classical' materials, where nonlinearity arises from atomic scale (nanoscopic scale). In case of more complex materials, either heterogeneous, cracked, or granular (mesoscopic scales), and for strain above roughly 10^{-6} [41,42], the Landau theory is not valid anymore[43,44]. Indeed, some typical behaviours appear in this case: an hysteresis with cusps is present in the stress-strain response, odd harmonics are favored, resonance frequency exhibits a linear shift with level of excitation[38], and a slow dynamic phenomenon appears[45,46]. The physical origins of these phenomena, which are still not completely understood, comes from a rearrangement of grains (dislocations, rupture, recovery bonds) which can be modeled as friction and/or clapping, together with a thermoelastic effect[47]. The 'hysteretic' regime (except slow dynamics effect) of these materials has been modeled phenomenologically by Guyer and McCall[48], using the Preisach-Mayergoyz Space (PM Space). In this model, materials are decomposed in hysteretic mesocopic units (HMU), which alternatively open and close at different pressure values. Equation 1 describing the nonlinear elastic modulus K in a one dimensional case can be derived from this model in the case of small acoustic strain, where a nonlinear nonclassical (or hysteretic) parameter α has been added to the nonlinear classical development of Landau (parameters β and δ of first and second order representing the quadratic and cubic nonlinearities respectively) :

$$K(\epsilon,\dot{\epsilon}) = K_0\left[1-\beta\epsilon-\delta\epsilon^2-\ldots-\alpha\left(\Delta\epsilon+sign(\dot{\epsilon})\,\epsilon\right)\right] \quad (1)$$

where K_0, ϵ, $\dot{\epsilon}$ and $\Delta\epsilon$ are the linear modulus, the strain, the time derivative of strain and the maximum strain excursion over a wave cycle, respectively. As the interface studied (threads) is at a mesoscopic scale, we expect to obtain a nonlinear hysteretic behaviour, where the parameter α dominates over δ. In this case, a first order approximation gives the equations 2 and 3[49]. Equation 2 leads to the nonlinear elastic parameter α_f (shift of the resonance frequency), whereas equation 3 leads to the nonlinear dissipative parameter α_ξ (damping variation):

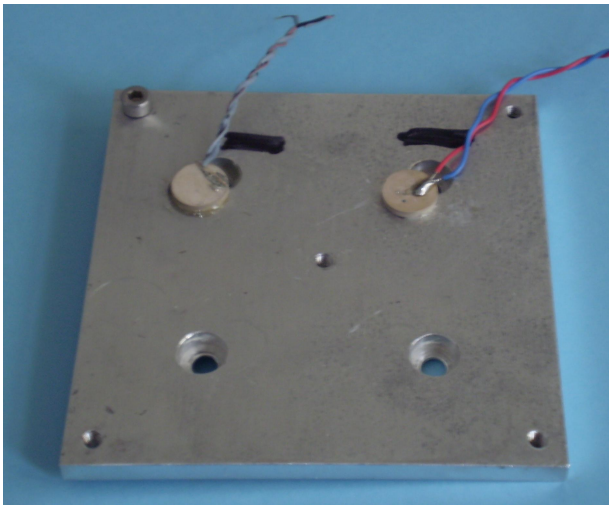

FIG. 1: Aluminum plate used in the experiment. A M4-screw is tightened in the upper left. Two piezoelectric sensors are bonded to the plate.

$$\frac{f-f_0}{f_0} = \alpha_f\epsilon \quad (2)$$

$$\frac{1}{Q}-\frac{1}{Q_0} = 2\xi-2\xi_0 = 2\xi_0\left(\frac{V\epsilon_0}{V_0\epsilon}-1\right) = \alpha_\xi\epsilon \quad (3)$$

where f, ξ, V and Q are the resonance frequency, the modal damping ratio, the voltage amplitude of excitation and the quality factor, respectively. The subscript "0" refers to the value obtained with the lowest amplitude of excitation (considered as a linear regime value). α_f and α_ξ are both proportional to the parameter α of equation 1. Equation 3 makes the assumption that strain is inversely proportional to the modal damping ratio[49]. This allows one to extract α_ξ without measuring ξ, an arduous problem in the frequency domain with a nonlinear regime.

III. MATERIAL AND METHODS

A. Material

Our system (fig. 1) is composed of a steel screw (M4, 16 mm-long) tightened at different torques (range 15-150 N.cm) in the corner of an aluminum plate (10×10 cm^2), using two dynamometric screwdrivers. The first screwdriver (Facom A.301MT) is used for torques between 15 and 75 N.cm, the second one (Facom A.402) is used for higher torques. Below 15 N.cm, the screw can be loosened by hand. We tighten until 150 N.cm, a value close to the maximum permissible value for this screw diameter (250 N.cm typically). The system is suspended by a string to obtain free boundary

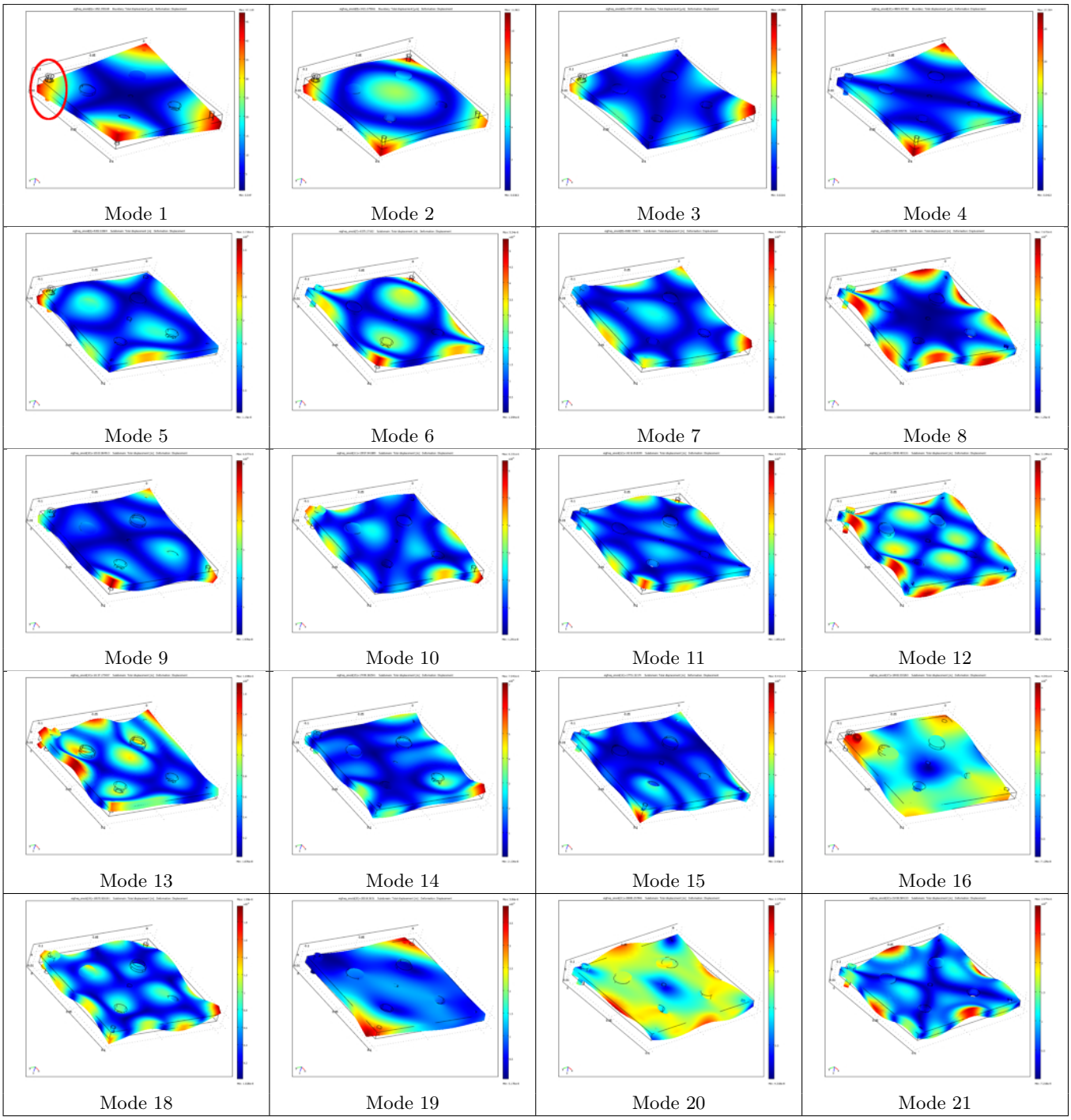

FIG. 2: Eigenmodes obtained by finite element modelling. The position of the screw is shown by the circle for mode 1. Color scale indicates the displacement field: blue zones (or dark on black and white versions) represent a zero displacement (or a maximum strain), and red zones (white zones and black and white versions) represent a maximum displacement (or a zero strain). Corresponding frequencies are shown on table I. Note that these modes mainly correspond to bending modes of the plate except modes n°16 and 19, which correspond to in-plane modes. Note also the absence of modes n°17 and 22, only present in the experiment.

n°	f_{exp} (Hz)	f_{mod} (Hz)	$\lvert f_{mod}-f_{exp}\rvert$ (Hz)	$\frac{\lvert f_{mod}-f_{exp}\rvert}{f_{exp}}$ (%)	Q_{exp} (.)
1	1846	1852	6	0.3	600
2	3447	3421	26	0.8	280
3	4665	4707	42	0.9	380
4	4832	4869	37	0.8	140
5	8140	8202	62	0.8	230
6	8373	8375	2	0.0	200
7	8567	8682	115	1.3	130
8	9369	9529	160	1.7	300
9	10330	10322	8	0.1	180
10	13800	13958	158	1.1	140
11	14010	14217	207	1.5	410
12	15600	15850	250	1.6	300
13	16040	16137	97	0.6	95
14	17300	17499	199	1.1	320
15	17450	17752	302	1.7	425
16	not excited	18402			not excited
17	19120	not detected			90
18	19380	19570	190	1.0	500
19	not excited	20319			not excited
20	20790	20880	90	0.4	380
21	21460	21459	1	0.0	290
22	23800	not detected			100

TABLE I: Comparison between experiment (f_{exp}) and finite element modelling (f_{mod}). The quality factor Q_{exp} is also given as information. All modes are identified except two (n°17 and 22), because of model's lacunae (cf text). Note also that two in-plane modes are obtained by FEM, but not excited in the configuration of the experiment (modes n°16 and 19).

conditions. Two piezoelectric sensors (PZT-5A, 12 mm diameter, 2 mm-thick) are bonded on the plate with glue, one is used as an emitter, the other as a receiver. The excitation is provided by a 14-bit waveform generator (Spectrum M2i6012) fed into a Tegam 2350 amplifier. The acquisition is performed applying a 14-bit Spectrum M2i4022 card.

B. Identification by FEM

The frequency range studied is 1-25 kHz. Beyond 25 kHz, density of modes is so great that they overlap and it becomes difficult to perform NRUS measurement on an isolated mode. These modes are identified with a Finite Element Model, using an eigenmode study (Comsol software). In this model, all geometrical characteristics are respected, except thread which is not represented. We model the contact plate/screw and plate/sensors as perfect (same displacement). Elastic

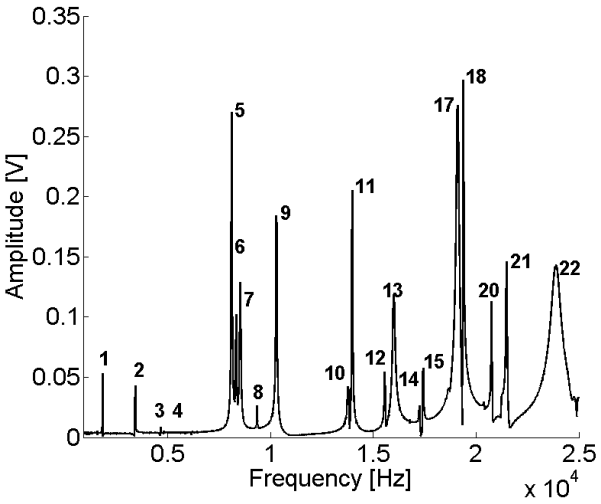

FIG. 3: Spectrum at 150N.cm in the range 1-25kHz. Each number corresponds to a mode in figure 2 and tables I and II.

characteristics included in the model for the aluminium plate, the steel screw and the PZT sensors are 70 GPa, 900 GPa and 70 GPa, respectively for the Young Modulus E, 2700 kg/m^3, 7850 kg/m^3 and 7750 kg/m^3, respectively for the density ρ. These values are typical from the literature and have not been matched to fit the experimental resonance frequencies. Moreover, the model does not include dissipative charateristics. Then, numerically obtained eigenfrequencies are compared to experimental ones, measured for the maximum torque (150N.cm in our case). Eigenmodes present in the range 1-25 kHz mainly correspond to bending modes of the plate (figure 2). These bending modes become more and more complex when frequency increases. Modes n°16 and 19 correspond to modes whose displacement field locates in the plane of the plate. These two modes are not present experimentally, as excitation favors out of plane modes. In table I, we note that identification by FEM is efficient, regarding absolute and relative differences between experiment (figure 3) and modelling. However, two modes present experimentally at 19.1 kHz and 23.8 kHz are not identified in the modelling (modes n°17 and 22 in table I). This poor identification can be explained by the fact that thread is not modeled at the interface screw/plate.

C. NRUS measurement

Each mode with linear resonance frequency f_0 is excited by a 1 s-long linear frequency sweep, whose starting and stopping frequencies correspond to $f_0 \pm 5\%$. The frequency sweep is then repeated for 30 increasing amplitudes of excitation. The linear parameters f_0 and ξ_0 are measured by fitting a lorentzian[49] to the resonance curve obtained for the lowest amplitude (considered as linear

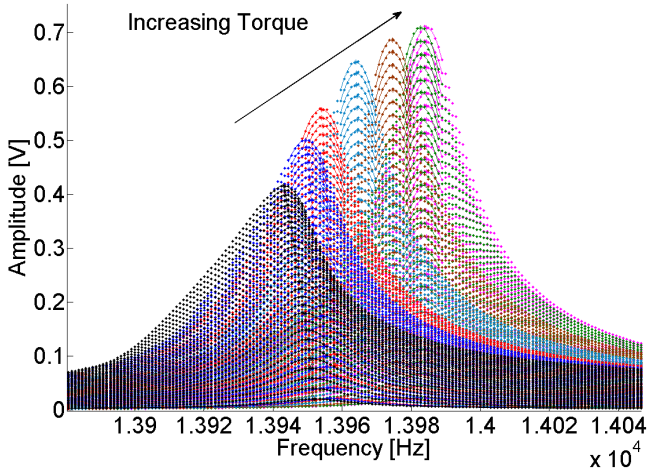

FIG. 4: Mode n°11 for 30 increasing amplitudes of excitation and 7 torques from 15 N.cm to 150 N.cm.

elastic). Resonance curves at higher amplitudes are fitted by a polynomial interpolation, allowing to extract the resonance frequency f and the corresponding amplitude. Finally, nonlinear elastic and dissipative parameters α_f and α_ξ are extracted for each mode, according to equations 2 and 3. This procedure is then repeated for increasing torques.

Experiments are performed in a temperature controlled room (25 ± 1 ℃). The duration time of 1 s for the frequency sweep has been chosen as a compromise between the possible heating of the system and achieving a steady-state at each frequency during the sweep. The characteristic time $\tau = Q/(\pi f_0)$, corresponding to 63 % of the exponential decrease of a free oscillator (with Q the quality factor of the mode) is in the worst configuration 10 times lower than the time excitation (1 s), meaning that the steady-state is reached at each frequency.

A waiting time between each excitation is needed to limit slow dynamics phenomenon from fast dynamics (NRUS) measurement. This waiting time was evaluated at the lowest torque (the case where nonlinearity is the highest). The resonance frequency of each mode is first measured with the weakest amplitude of excitation. Then, the system is excited with a 1 s-long excitation at the highest amplitude used in the measurement. Just after, the resonance frequency is measured again with the weakest amplitude. Therefore, it appears that approximately 10 s are needed for the system to recover its original resonance frequency. We make the assumption that this characteristic time is the worst case (longest duration slow dynamics) and therefore this rest time is applied between each excitation.

Finally, the NRUS experiment is repeated three times (with repositioning of the screw) and displayed error bars represent 2 standard deviations.

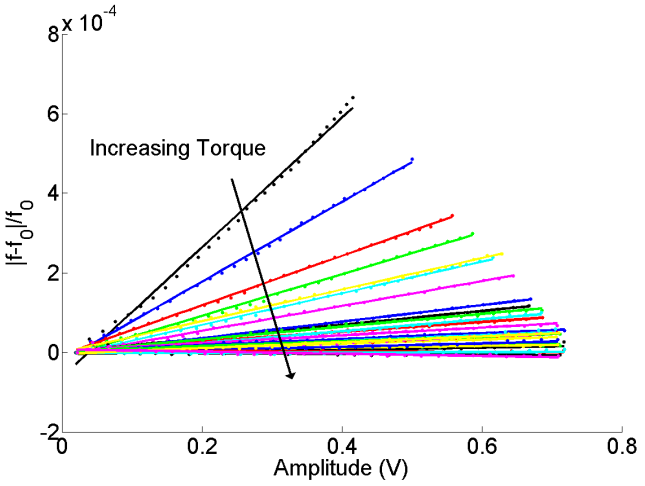

(a)

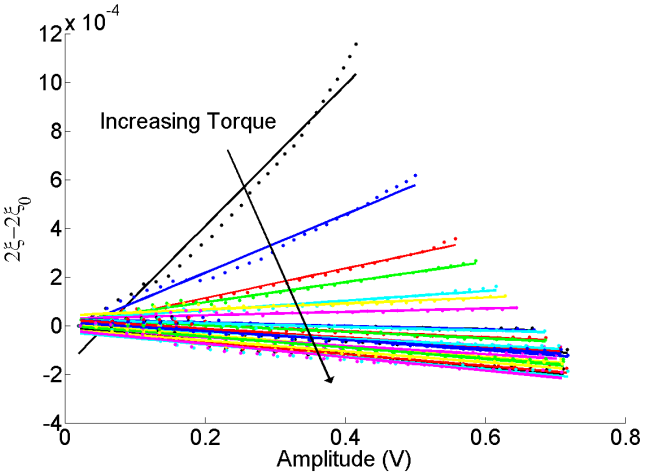

(b)

FIG. 5: **(a)** Relative frequency shift $|f - f_0|/f_0$ of mode n°11 versus voltage amplitude of detector (proportional to strain) for 28 increasing torques. Each curve is linearly fitted and the slope obtained corresponds to the parameter $C\alpha_f$ with C a constant. **(b)** Damping variation $2\xi - 2\xi_0$ of mode n°11 versus voltage amplitude of detector (proportional to strain) for 28 increasing torques. Each curve is linearly fitted and the slope obtained corresponds to the parameter $C\alpha_\xi$ with C a constant.

IV. RESULTS

Modes in the range 1 to 10 kHz (n°1 to 9) exhibit weak nonlinearity and little sensitivity to torque changes. Then, most of modes in the range 10-25 kHz exhibit higher nonlinearities at low torques. As an example, we can observe in figure 4 the typical behaviour of mode n°11 for 30 amplitudes, and 7 torques from 15 to 150 N.cm. In this figure, we can observe qualitatively that the higher the torque, the higher the resonance frequency. Moreover, increasing torque leads to higher

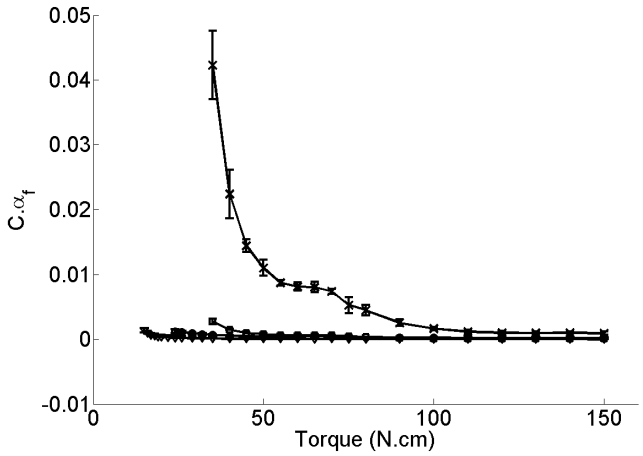

(a)

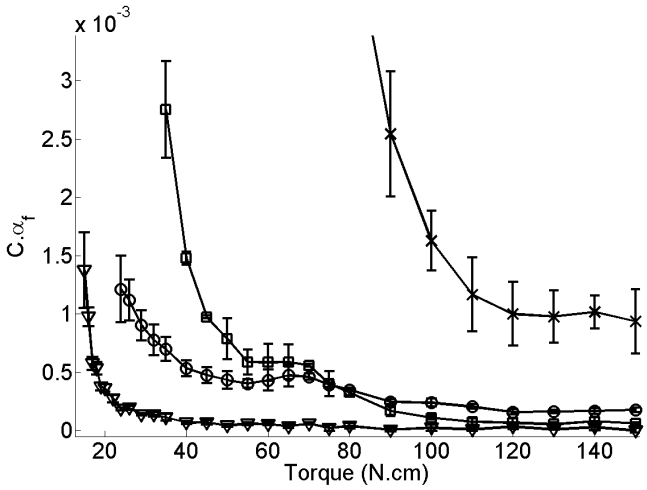

(b)

FIG. 6: **(a)** Nonlinear elastic parameter Cα_f as a function of torque for modes n°11 (▽),20 (□),21 (○) and 22 (×), where C is a constant. Mode n°11 is present in the spectrum over the entire torque range, while modes 20, 21 and 22 appear at torque 35, 24 and 35 N.cm respectively. **(b)** Zoom of (a) on modes 20, 21 and 22.

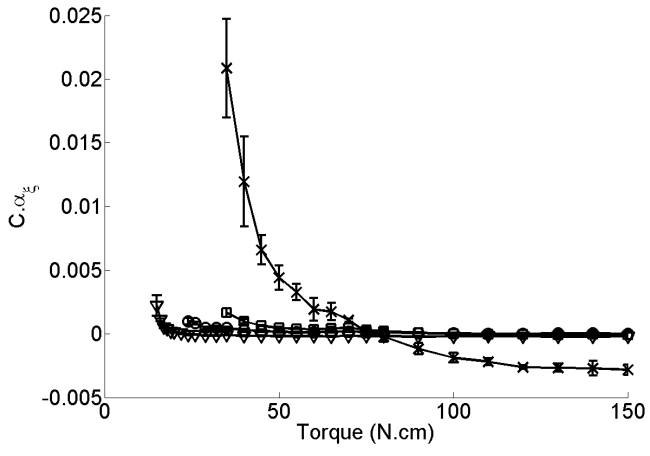

(a)

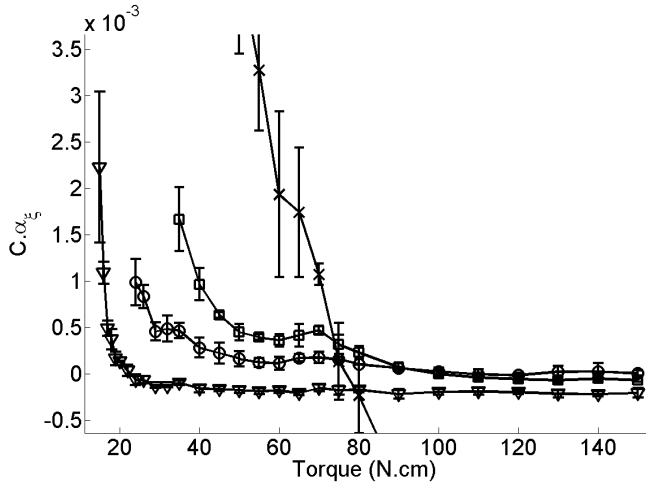

(b)

FIG. 7: **(a)** Nonlinear dissipative parameter Cα_ξ as a function of torque for modes n°11 (▽), 20 (□), 21 (○) and 22 (×), where C is a constant. Mode n°11 is present in the spectrum over the entire torque range, while modes 20, 21 and 22 appear at torque 35, 24 and 35 N.cm respectively. **(b)** Zoom of (a) on modes 20, 21 and 22.

amplitudes and lower damping. Finally, the frequency shift decreases (the slope tends to be vertical). This seems logical with our understanding of the system. Indeed, as a first approximation, if we consider the most elementary vibrational system (generally termed mass-spring system), with a mass m and a stiffness k, the resonance frequency of this system will be $f = \frac{1}{2\pi}\sqrt{k/m}$. In this system, f is proportional to $\sqrt{k}$ and that is what we observe when increasing torque: stiffness increases for a same mass. Likewise, the contact screw/plate is more and more stressed when increasing torque. Thus, linear dissipation and elastic nonlinearity are more present for low torques, as observed in figure 4, where linear dissipation induces 'broader' modes and lower amplitudes and elastic nonlinearity induces higher frequency shift with drive amplitude. Quantitatively, these phenomena are represented from figures 5 to 9. Figure 5, the relative frequency shift $|f - f_0|/f_0$ and damping variation $2\xi - 2\xi_0$ are plotted versus voltage amplitude received by the detector sensor. In this figure, each curve is linearly fitted and the slope of each fit corresponds to Cα_f and Cα_ξ, with C a constant (the amplitude in Volts is proportional to strain). This slope decreases dramatically when torque increases, meaning that the system tends toward a linear regime.

In figures 6 and 7, we can observe the behaviour of nonlinear elastic and dissipative parameters respectively for 4 modes. Mode n°11 is present in the spectrum over the entire torque range, while modes 20, 21 and

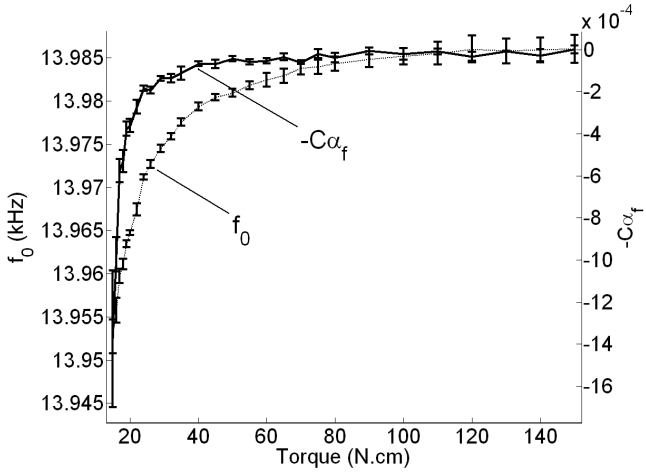

FIG. 8: Mode n°11. Evolution of linear (f_0 in dashed line) and nonlinear (-Cα_f in bold line) elastic parameters *vs* torque. The opposite value of Cα_f is plotted to allow the sensitivity comparison.

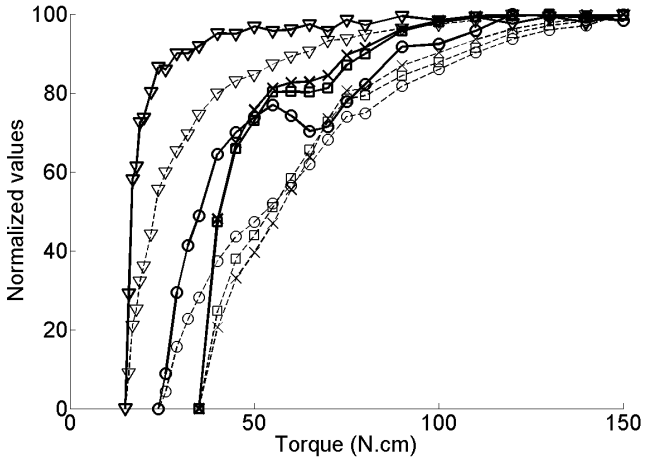

FIG. 9: Normalized values from 0 to 100 for linear (f_0 in dashed line) and nonlinear (-Cα_f in bold line) elastic parameters of modes n°11 (∇), 20 ($\square$), 21 ($\circ$) and 22 ($\times$). The opposite value of Cα_f is plotted to allow the sensitivity comparison.

22 appear at torques about 35, 24 and 35 N.cm respectively. Actually, these modes appear progressively in the spectrum when increasing torque and below these torque values, the signal to noise ratio is too weak to perform a reliable measurement. Modes 20, 21 and 22, appearing during tightening, can be considered as new events in the spectrum and are very useful to follow. Indeed, their sensitivity is great at the beginning of their torque range. Thus, combination of modes allows one to maintain sensitivity over the entire torque range. In figures 6 and 7, we also notice that the mode 22 is much more sensitive than others. It was not detected by FEM, certainly due to a poor representation of thread in the model.

Figure 8 compares linear and nonlinear elastic parameters for the mode n°11. It appears that nonlinear elastic parameter is sensitive at the beginning of the torque range (from 15 to 40 N.cm) while linear elastic parameter is sensitive from 15 to 80 N.cm. However, when the nonlinear parameter is sensitive, it is more sensitive than linear one. Beyond the sensitivity level of each parameter, the nonlinear parameter brings some new information on the system, complementary to the linear one. This point will be developed more in-depth in the discussion part.

Finally, figure 9 displays normalized values of linear and nonlinear elastic parameters for modes 11, 20, 21 and 22. When sensitive, the nonlinear parameter of each mode is more sensitive than its linear counterpart. Therefore, the addition of modes implies that the nonlinear method is more sensitive than the linear frequency change. An equivalent comparison can be made between linear and nonlinear dissipative parameters. The behaviour is highly similar, even if modal damping ratio (linear parameter) is more artefacted by the presence of adjacent modes.

Modes 12 and 15 are also sensitive to torque variations, and exhibit a behaviour similar to the mode 11 (good sensitivity between 15 and 40 N.cm). They are not displayed here in order to keep a clear presentation of results. Modes 10 and 13 exhibit a weak nonlinearity and a little sensitivity to torque changes. Mode 14 has very low energy (figure 3), so that the signal to noise ratio is too weak to perform a consistent measurement. Finally, modes 17 and 18 overlap at lowest torques (from 15 to about 35 N.cm). A measurement is nevertheless possible above 35 N.cm and exhibits good sensitivity to torque changes.

In this study, it appears that sensitive modes have a nodal line of displacement "passing" over the screw (11, 12, 15, 18, 20, 21 and except 18) whereas insensitive modes 10 and 13 do not. This nodal line corresponds to a maximum strain, and it seems logical that this maximum strain favors strong sensitivity. However, modes at lower frequency, for example n°6 or 8, present a similar nodal line but are not sensitive. We can not answer clearly about this insensitivity but we can speculate that they may be sensitive at torques lower than 15 N.cm. These results are summed up in the table II.

V. DISCUSSION

The main purpose of this study was to show that nonlinear resonance ultrasound spectroscopy was sensitive to tightening forces of an interface screw/plate. We show that this nonlinear method provide a sensitive parameter α. A comparison is made between linear

n°	Frequency (HZ)	Torque range of existence (N.cm)	Torque range of sensitivity for α_f (N.cm)	Torque range of sensitivity for α_ξ (N.cm)	Nodal line on the bolt
1	1846	15-150	very weak	very weak	no
2	3447	15-150	very weak	very weak	no
3	4665	15-150	very weak	very weak	no
4	4832	15-150	very weak	very weak	yes
5	8140	15-150	very weak	very weak	no
6	8373	15-150	very weak	very weak	yes
7	8567	15-150	very weak	very weak	no
8	9369	15-150	very weak	very weak	yes
9	10330	15-150	very weak	very weak	no
10	13800	15-150	very weak	very weak	no
11	14010	15-150	15-40	15-30	yes
12	15600	15-150	15-40	15-40	yes
13	16040	15-150	very weak	very weak	no
14	17300	15-150	very weak	very weak	no
15	17450	15-150	15-40	15-40	yes
16	not excited				
17	19120	15-150	overlapping with 18	overlapping with 18	not detected
18	19380	15-150	overlapping with 17	overlapping with 17	no
19	not excited				
20	20790	35-150	35-120	35-120	yes
21	21460	24-150	24-120	24-120	yes
22	23800	35-150	35-110	35-120	not detected

TABLE II: Summary of results obtained for each mode. Torque range of sensitivity for α_f and α_ξ are displayed, as well as the presence of a nodal line of displacement on the screw (corresponding to a maximum strain).

and nonlinear parameters. It appears that nonlinear parameters are sensitive over a narrower torque range but are more sensitive than linear parameters in this range. Furthermore, by following several modes in the spectrum and by analyzing modes which are not present in the entire torque range, we are able to increase the sensitivity range of the nonlinear approach. This could be implemented in a future as a 'nonlinear modal analysis'.

A. Multimodal NRUS measurement

This study constitutes one of the rare systematic multimodal NRUS measurement. Therefore, we remark on several points. Each mode have to be isolated from adjacent ones to avoid artefacts in the analysis, especially for dissipative parameters. Hence, modes at relatively low frequency are generally the most suitable, as the mode density is low. Moreover, the system geometry has to be as asymmetric as possible, to avoid several eigenmodes around the same frequency. We also observe that the most suitable configuration to perform a measurement occurs when emittor and detector are placed on a strain node (or a maximum displacement), which favours an energetic mode, while the source of nonlinearity is placed on a displacement node (or a maximum strain), which favours a sensitive mode. Also, when the source of nonlinearity remains unknown, sensitivity or insensitivity of different modes allows one to localize it[39].

B. Measurement artefacts

We noted previously that for the highest torques, slopes are slightly negative in figure 5(b), leading to negative α_ξ values: they correspond to a transparency effect[50]. Moreover, when performing the experiment without the screw, the nonlinear dissipative parameter is also slightly negative and with similar values. This behaviour, which was not expected, could come from electronic devices, bonding of piezoelectric sensors, and/or geometric nonlinearity.

C. Physical modelling and nonlinearity origins

For lowest torques (figure 5), the evolution of the relative frequency shift and damping variation of mode n°11 does not seem to be linear but rather quadratic. Thus, by fitting a second order polynomial on these curves, it appears that a combination of δ and α (cubic and hysteretic nonlinearities respectively) is more appropriate, reflecting the coexistence of classical and hysteretic regimes simultaneously. Nevertheless, a coarse linear fit allows to compare a same parameter over the entire torque range.

Furthermore, this study points out a need for a model to characterize the nonlinear behaviour of a screw/plate interaction under acoustic wave excitation, and beyond the PM space formalism presented in part II. The nonlinear behaviour of the system comes from the interface between the screw and the plate. Indeed, and similarly to rocks where grains (rigid system) are interconnected with softer bondings, the interface screw/plate can be considered as a soft object between two rigid objects (screw and plate themselves). Then, nonlinearity level will depend on static forces present at the interface, the roughness of both surfaces, the presence of a liquid, etc. This model would have to describe (1) the coexistence of classical and hysteretic regimes at lower torques (2) a decrease of both nonlinear parameters with increasing torque until the linear regime, with a faster decrease for the classical parameter.
As a starting point, asperities at the interface could be modelled as micro-spheres in contact, and described by a Hertzian nonlinearity. Indeed, this model could describe the presence of classical regime at low torques. This model allows one to describe the contact between two unconsolidated spheres under normal forces, giving a classical nonlinear elasticity[51]. Then, models derived from the Hertz-Mindlin theory take into account both normal and tangential forces and the possibility of a stick/slip behaviour. The latter leads to a hysteretic regime[52] and could be efficient to describe a screw/plate interaction at higher torques.

D. Strain level

The strain level applied by the acoustic wave to thread remains unknown (nonlinear parameters obtained are not α_f and α_ξ, but $C\alpha_f$ $C\alpha_\xi$, with a constant C). However, by using piezoelectric characteristics of sensors used in the experiment, we are able to obtain an order of magnitude for strain applied to the system. Indeed, strain applied to the emittor is between 10^{-6} and 5.10^{-5} for the lowest and highest amplitudes of excitation respectively, while the strain received by the detector is between 5.10^{-9} and 10^{-7}. This evaluation does not give strain values received by the interface screw/plate, but values of this order are speculated.

VI. CONCLUSIONS

The main purpose of this study was to show that nonlinear resonance ultrasound spectroscopy was sensitive to tightening forces of an interface screw/plate. Nonlinear parameters appear to be a useful tool to characterize a thread interaction, complementary to linear ones. We also show that a multimodal study allows to increase the torque range of sensibility. The study will be carried on in the future by both academic works and medical or industrial applications.

* Electronic address: jacques.riviere@upmc.fr
† Electronic address: paj@lanl.gov

[1] F. R. Rollins. Ultrasonic analysis of bolt loads. *IEEE transactions on sonics and ultrasonics*, SU18:46–&, 1971.
[2] H. J. Mcfaul. Ultrasonic device to measure high-strength bolt preloading. *Materials Eval.*, 32:244–248, 1974.
[3] J. S. Heyman. CW ultrasonic bolt-strain monitor. *Exp. Mech.*, 17:183–187, 1977.
[4] J. F. Smith and J. D. Greiner. Stress measurement and bolt tensioning by ultrasonic methods. *J. of Metals*, 32:34–36, 1980.
[5] S. A. Nassar and A. B. Veeram. Ultrasonic control of fastener tightening using varying wave speed. *J. Pressure Vessel Technol.*, 128:427–432, 2006.
[6] S. Chaki, G. Corneloup, I. Lillamand, and H. Walaszek. Nondestructive control of bolt tightening: Absolute and differential evaluation. *Materials Eval.*, 64:629–633, 2006.
[7] T. Zweschper, A. Dillenz, and G. Busse. Ultrasound lock-in thermography - a defect-selective NDT method for the inspection of aerospace components. *Insight*, 43:173–179, 2001.
[8] T. Zweschper, A. Dillenz, and G. Busse. NDE of adhesive joints and riveted structures with lock-in thermography methods. Proc. SPIE, pages 567–573, 2001.
[9] M. Morozov, G. Rubinacci, A. Tamburrino, S. Ventre, and F. Villone. Novel fluxset sensor based EC probe for crack detection in aluminium rivet joints. In *Electromagn. Nondestr. Eval. (IX)*, volume 25, pages 195–202, 2005.
[10] S. Paillard, G. Pichenot, M. Lambert, H. Voillaume, and N. Dominguez. A 3D model for eddy current inspection in aeronautics: Application to riveted structures. In *Rev. Progress Quantitative Nondestr. Eval.*, volume 894 of *Proc. AIP*, pages 265–272, 2007.
[11] Y. Le Diraison, PY. Joubert, and D. Placko. Characterization of subsurface defects in aeronautical riveted lap-joints using multi-frequency eddy current imaging. *NDT & E Int.*, 42:133–140, 2009.
[12] N. Raghu, V. Anandaraj, K. V. Kasiviswanathan, and P. Kalyanasundaram. Neutron radiographic inspection of industrial components using Kamini neutron source facility. volume 989 of *Proc. AIP*, pages 202–205, 2008.
[13] J. R. Tarpani, A. H. Shinohara, V. Swinka Filho, R. R. da Silva, and N. V. Lacerda. Digital versus Conventional Radiography for Imaging Fatigue Cracks in Riveted Lap Joints of Hybrid Glass Reinforced Fiber/Metal Laminate. *Materials Eval.*, 66:1279–1286, 2008.
[14] M. Cacciola, Y. Deng, F. C. Morabito, L. Udpa, S. Udpa, and M. Versaci. Automatic fuzzy based identification of flawed rivet in Magneto Optic Images. *Int. J. Appl. Electromagn. Mech.*, 28:297–303, 2008.
[15] PY. Joubert and J. Pinassaud. Linear magneto-optic imager for non-destructive evaluation. *Sensors Actuat. A*, 129:126–130, 2006.
[16] N. Meredith, D. Alleyne, and P. Cawley. Quantitative de-

termination of the stability of the implant-tissue interface using resonance frequency analysis. *Clinical Oral Implants Res.*, 7:261–267, 1996.

[17] B. Dhoedt, D. Lukas, L. Muhlbradt, F. Scholz, W. Schulte, F. Quante, and A. Topkaya. Periotest procedure - development and clinical-testing. *Deutsche Zahnarztliche Zeitschrift*, 40:113–125, 1985.

[18] A. Zagrai, D. Doyle, and B. Arritt. Embedded nonlinear ultrasonics for structural health monitoring of satellite joints. volume 6935 of *Proc. SPEI*, page 93505, 2008.

[19] D. Doyle, A. Zagrai, B. Arritt, and H. Cakan. Damage detection in satellite bolted joints. In *Proc. ASME*, pages 209–218, 2009.

[20] I. Solodov, K. Pfleiderer, H. Gerhard, S. Predak, and G. Busse. New opportunities for NDE with air-coupled ultrasound. *NDT & E Int.*, 39:176–183, 2006.

[21] P. A. Johnson, T. J. Shankland, R. J. Oconnell, and J. N. Albright. Nonlinear generation of elastic-waves in crystalline rock. *Journal of Geophysical Research-Solid Earth and Planets*, 92:3597–3602, 1987.

[22] P. A. Johnson, B. Zinszner, and P. N. J. Rasolofosaon. Resonance and elastic nonlinear phenomena in rock. *Journal of Geophysical Research-Solid Earth*, 101:11553–11564, 1996.

[23] J.Y. Kim, L.J. Jacobs, J. Qu, and J.W. Littles. Experimental characterization of fatigue damage in a nickel-base superalloy using nonlinear ultrasonic waves. *J. Acoust. Soc. Am.*, 120:1266, 2006.

[24] K. Van den Abeele and J. De Visscher. Damage assessment in reinforced concrete using spectral and temporal nonlinear vibration techniques. *Cem. Concr. Res.*, 30:1453–1464, 2000.

[25] J.A. TenCate. New nonlinear acoustic techniques for nde. *Rev. Prog. Quant. Nondestr. Eval.*, 557:1229–1235, 2001.

[26] C. Payan, V. Garnier, J. Moysan, and P. A. Johnson. Applying nonlinear resonant ultrasound spectroscopy to improving thermal damage assessment in concrete. *J. Acoust. Soc. Am.*, 121:125–130, 2007.

[27] V. Bucur and P. N. J. Rasolofosaon. Dynamic elastic anisotropy and nonlinearity in wood and rock. *Ultrasonics*, 36:813–824, 1998.

[28] M. Muller, A. Sutin, R. Guyer, M. Talmant, P. Laugier, and P. A. Johnson. Nonlinear resonant ultrasound spectroscopy (nrus) applied to damage assessment in bone. *J. Acoust. Soc. Am.*, 118:3946–3952, 2005.

[29] T. J. Ulrich, P. A. Johnson, M. Muller, D. Mitton, M. Talmant, and P. Laugier. Application of nonlinear dynamics to monitoring progressive fatigue damage in human cortical bone. *Appl. Phys. Lett.*, 91, 2007.

[30] W.L. Morris, O. Buck, and R. V. Inman. Acoustic harmonic-generation due to fatigue damage in high-strength aluminum. *J. Appl. Phys.*, 50:6737–6741, 1979.

[31] I. Y. Solodov, A. F. Asainov, and S. L. Ko. Nonlinear saw reflection - experimental-evidence and nde applications. *Ultrasonics*, 31:91–96, 1993.

[32] S. Biwa, S. Hiraiwa, and E. Matsumoto. Experimental and theoretical study of harmonic generation at contacting interface. *Ultrasonics*, 44:1319–1322, 2006.

[33] K. E. A. Van den Abeele, P.A. Johnson, and A. Sutin. Nonlinear elastic wave spectroscopy (NEWS) techniques to discern material damage, part I: Nonlinear wave modulation spectroscopy (NWMS). *Res. Nondestr. Eval.*, 12:17–30, 2000.

[34] I. Solodov, J. Wackerl, K. Pfleiderer, and G. Busse. Nonlinear self-modulation and subharmonic acoustic spectroscopy for damage detection and location. *Appl. Phys. Lett.*, 84:5386–5388, 2004.

[35] V. Zaitsev, V. Gusev, and B. Castagnede. Luxemburg-Gorky effect retooled for elastic waves: A mechanism and experimental evidence. *Phys. Rev. Lett.*, 89:607–613, 2002.

[36] B. Mi, J. E. Michaels, and T. E. Michaels. An ultrasonic method for dynamic monitoring of fatigue crack initiation and growth. *J. Acoust. Soc. Am.*, 119:74–85, 2006.

[37] G. Renaud, S. Calle, and M. Defontaine. Remote dynamic acoustoelastic testing: Elastic and dissipative acoustic nonlinearities measured under hydrostatic tension and compression. *Appl. Phys Lett.*, 94, 2009.

[38] K. E. A. Van den Abeele, J. Carmeliet, J. A. Ten Cate, and P. A. Johnson. Nonlinear elastic wave spectroscopy (NEWS) techniques to discern material damage, Part II: Single-mode nonlinear resonance acoustic spectroscopy. *Res. Nondestr. Eval.*, 12:31–42, 2000.

[39] K. Van Den Abeele. Multi-mode nonlinear resonance ultrasound spectroscopy for defect imaging: An analytical approach for the one-dimensional case. *J. Acoust. Soc. Am.*, 122:73–90, 2007.

[40] L.D. Landau and E.M. Lifshitz. *Theory of Elasticity, Third Edition (Theoretical Physics, Vol 7)*. Butterworth-Heinemann, 1986.

[41] J. A. TenCate, D. Pasqualini, S. Habib, K. Heitmann, D. Higdon, and P. A. Johnson. Nonlinear and nonequilibrium dynamics in geomaterials. *Phys. Rev. Lett.*, 93, 2004.

[42] D. Pasqualini, K. Heitmann, J. A. TenCate, S. Habib, D. Higdon, and P. A. Johnson. Nonequilibrium and nonlinear dynamics in berea and fontainebleau sandstones: Low-strain regime. *J. Geophys. Res.*, 112, 2007.

[43] L. K. Zarembo and V. A. Krasil'nikov. Nonlinear phenomena in propagation of elastic waves in solids. *Sov. Phys. Usp.*, 13:778–&, 1971.

[44] L. A. Ostrovsky, I. A. Soustova, and A. M. Sutin. Nonlinear and parametric phenomena in dispersive acoustic systems. *Acustica*, 39:298–306, 1978.

[45] J. A. TenCate and T. J. Shankland. Slow dynamics in the nonlinear elastic response of berea sandstone. *Geophys. Res. Lett.*, 23:3019–3022, 1996.

[46] R. A. Guyer, K. R. McCall, and K. Van Den Abeele. Slow elastic dynamics in a resonant bar of rock. *Geophys. Res. Lett.*, 25:1585–1588, 1998.

[47] V. Gusev and V. Tournat. Amplitude- and frequency-dependent nonlinearities in the presence of thermally-induced transitions in the preisach model of acoustic hysteresis. *Phys. Rev. B*, 72, 2005.

[48] R. A. Guyer, K. R. McCall, and G. N. Boitnott. Hysteresis, discrete memory, and nonlinear-wave propagation in rock - a new paradigm. *Phys. Rev. Lett.*, 74:3491–3494, 1995.

[49] P. Johnson and A. Sutin. Slow dynamics and anomalous nonlinear fast dynamics in diverse solids. *J. Acoust. Soc. Am.*, 117:124–130, 2005.

[50] V Gusev and VY Zaitsev. Acoustic dither injection in a medium with hysteretic quadratic nonlinearity. *Phys. Lett. A*, 314:117–125, 2003.

[51] L. Ostrovsky and P.A. Johnson. Dynamic nonlinear elasticity in geomaterials. *Riv. Nuovo Cimento*, 24:1–46, 2001.

[52] V. Aleshin and K. Van Den Abeele. Preisach analysis of the Hertz-Mindlin system. *J. Mech. Phys. Solids*, 57:657–672, 2009.